

# 1D Modeling of LHD Divertor Plasma and Hydrogen Recycling

Gakushi KAWAMURA<sup>1)</sup>, Yukihiro TOMITA<sup>1)</sup>, Masahiro KOBAYASHI<sup>1)</sup> and David TSKHAKAYA<sup>2,3)</sup>

<sup>1)</sup>National Institute for Fusion Science, Gifu 509-5292, Japan

<sup>2)</sup>Association Euratom-ÖAW, Institute of Theoretical Physics, University of Innsbruck, Technikerstrasse 25/II, Innsbruck A-6020, Austria

<sup>3)</sup>Permanent address: Institute of Physics, Georgian Academy of Sciences, 380077 Tbilisi, Georgia

(Received 9 January 2009 / Accepted 16 May 2009)

One dimensional plasma and neutral model of the divertor plasma in Large Helical Device is presented. The plasma is described by stationary fluid equations for electron and ion. The atomic processes such as dissociation of hydrogen molecules released from the divertor plate, ionization of hydrogen atoms, charge exchange and recombination are included in equations of neutrals. This model is intended to be employed in an integrated simulation where an equilibrium of the upstream plasma and plasma-surface interactions at the divertor plate are solved in different numerical codes separately. From the computational point of view, the numerical code for the divertor plasma is developed for 1D flux tube where the boundary conditions of both ends are specified. The calculation time is less than one second and reasonably short to use in future integrated simulations. In the results, interactions between plasma and neutrals and dependence of the energy loss on the plasma density are studied. In low density case, the energy is lost through ionization and charge exchange but the total amount of the loss is small and the impurity loss is negligibly small. In high density case, the ionization loss and impurity cooling become much larger than the charge exchange loss and causes a drop of the heat flux.

© 2010 The Japan Society of Plasma Science and Nuclear Fusion Research

Keywords: LHD, divertor, fluid, neutral, recycling

DOI: 10.1585/pfr.5.S1020

## 1. Introduction

The Large Helical Device (LHD) [1] is a heliotron/teratron type device with helical divertors. A poloidal cross section is illustrated in Fig. 1. The LHD plasma has an ergodic layer [2], i.e. region 'A' in Fig. 1, outside the core plasma. The divertor leg plasma, i.e. region 'B' in Fig. 1, is connected to the ergodic layer and parallel flow along the magnetic field is dominant there. The plasma profiles such as density and temperature determine dynamics and charge state of impurities, which causes undesirable radiation cooling in the core plasma. Therefore, physical understandings of the divertor plasma and its modeling for simulation studies on LHD boundary plasmas are important issues.

In this paper, we present plasma and neutral models of the divertor plasma to determine the plasma and neutral profiles which are characterized by input parameters such as heat flux coming from the ergodic layer and the plasma density at the upstream boundary. The model presented here is intended to be employed in our future simulation studies as a model of divertor legs to connect the following two simulation codes; EMC3 code [2] for the ergodic layer and ERO code [3] for the plasma-surface interactions at the divertor. The former code solves fluid equations to obtain equilibrium plasma profiles in the stochastic magnetic field and the latter solves impurity's equations

of motion to obtain the sputtering yield, time evolution of surface conditions and impurity transport near a target plate. EMC3 code employs a field-aligned mesh to reduce calculation time and keep the stochastic characteristic of the magnetic fields. A strong magnetic shear in the LHD boundary plasma, however, causes a difficulty in generation of the mesh, especially near the divertor legs. In order to avoid the numerical difficulty and to keep the amount of the computational resources in reasonable level, we developed a 1D model along the magnetic field line, i.e. a flux tube model, to extend the plasma region of EMC3 code to the divertor legs.

The plasma fluid equations are described in Sec. 2.1.

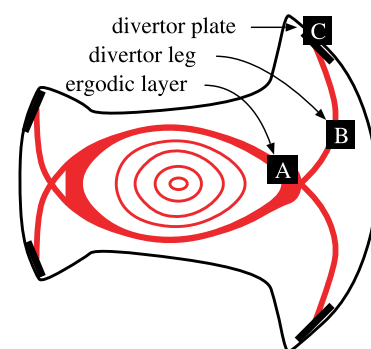


Fig. 1 Schematic illustration of a poloidal cross section of LHD.

They include interaction with neutrals and impurity cooling [4–7]. The differences of our model from those of precedent works are the neutral equations discussed in Sec. 2.2, which includes atomic processes such as dissociation and ionization of hydrogen molecules and atoms. In Sec. 3, comparisons with our previous model [8] and discussion of heat flux and energy loss are given. Finally in Sec. 4, conclusions are presented.

## 2. Divertor Plasma and Neutral Models

### 2.1 Fluid equations of plasma

We use Braginskii-type two fluid equations [9] to describe the divertor plasma. Since 1D fluid equations along the magnetic field and the method of numerical solution was given in the previous paper [8], we summarize them briefly here. We denote the plasma density, velocity, electron and ion temperatures and electrostatic potential by  $n(s)$ ,  $v(s)$ ,  $T_e(s)$ ,  $T_i(s)$  and  $\phi(s)$ , respectively. The position along the magnetic field is described by  $s$  and has zero value,  $s = 0$ , at the upstream boundary and the plasma length,  $s = l_p$ , at the entrance of the magnetic presheath [10]. The four balance equations of density, momentum, temperatures and force are given by

$$\frac{dnv}{ds} = S_n, \quad (1)$$

$$\frac{d}{ds} [m_i n v^2 + n(T_e + T_i)] = S_p, \quad (2)$$

$$\frac{d}{ds} \left[ \frac{5}{2} n v T_e - \kappa_e \frac{dT_e}{ds} \right] = S_{Ee} + env \frac{d\phi}{ds} - \frac{3m_e n}{m_i \tau_e} (T_e - T_i) - L r_{imp} n^2, \quad (3)$$

$$\frac{d}{ds} \left[ \frac{m_i n v^3}{2} + \frac{5n v T_i}{2} - \kappa_i \frac{dT_i}{ds} \right] = S_{Ei} - env \frac{d\phi}{ds} + \frac{3m_e n}{m_i \tau_e} (T_e - T_i), \quad (4)$$

$$\frac{1}{n} \frac{dnT_e}{ds} + 0.71 \frac{dT_e}{ds} - e \frac{d\phi}{ds} = 0, \quad (5)$$

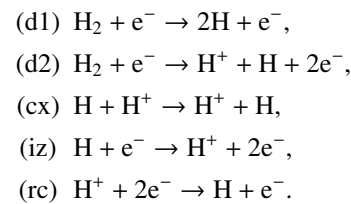
where electron and ion mass, carbon impurity ratio, radiative cooling rate coefficient, heat conduction coefficients were denoted by  $m_e$ ,  $m_i$ ,  $r_{imp}$ ,  $L$ ,  $\kappa_e = 3.16n\tau_e T_e/m_e$  and  $\kappa_i = 3.9n\tau_i T_i/m_i$  [11]. Electron and ion collision times are given by  $\tau_e = 6\sqrt{2}\pi^{3/2}\epsilon_0^2\sqrt{m_e}T_e^{3/2}/e^4n\ln\Lambda$  and  $\tau_i = 12\pi^{3/2}\epsilon_0^2\sqrt{m_i}T_i^{3/2}/e^4n\ln\Lambda$ , respectively. Permittivity, elementary charge and coulomb logarithm is denoted by  $\epsilon_0$ ,  $e$  and  $\ln\Lambda$ , respectively. Particle flux, pressure, electron and ion heat fluxes, i.e. left-hand side of each equation, are denoted by  $G$ ,  $P$ ,  $Q_e$  and  $Q_i$  in the remaining sections, respectively. The source terms associated with neutrals in the right-hand side, i.e.  $S_n$ ,  $S_p$ ,  $S_{Ee}$  and  $S_{Ei}$ , are given later in Sec. 2.2. The following conditions and relations are assumed in these equations; i) the temperature anisotropy time is negligibly short compared with the particle dwell time, i.e.  $T_\perp = T_\parallel = T$ , ii) ambipolar flow, i.e.  $v_e = v_i = v$ ,

iii) quasineutral condition, i.e.  $n_e = n_i = n$ . The conditions ii) and iii) imply the existence of bipolar electric fields and the absence of current along the magnetic fields.

In this paper, we use variables with subscripts '0' and '1' to indicate boundary values at  $s = 0$  and  $l_p$ , respectively. The plasma equations, Eqs. (1)–(5), are integrated numerically from the wall to the upstream boundary. Since our model is intended to be employed to connect different simulation codes at  $s = 0$  and  $l_p$ , the plasma density and heat flux at the upstream boundary are treated as free parameters. The integral of the plasma equations, however, requires boundary values at  $s = l_p$  as initial values. Therefore we utilize the multi-dimensional Newton's method to determine the initial values satisfying the density and heat flux at  $s = 0$  and the following three conditions; i) equality of the Bohm criterion at  $s = l_p$ , i.e.  $v_1 = c_s \equiv \sqrt{(T_{e1} + T_{i1})/m_i}$ , ii) potential  $\phi_1 = 0$ , iii) electron and ion heat fluxes at  $s = l_p$  determined by the sheath theory [8, 11].

### 2.2 Modeling of neutrals

In order to include interactions of plasma, hydrogen molecules and atoms, we choose five dominant reactions in the divertor plasma.



The first and second reactions, (d1) and (d2), represent the dissociation of hydrogen molecules to atoms. The reaction (d2) consists of two reactions,  $\text{H}_2 + e^- \rightarrow \text{H}_2^+ + 2e^-$  and  $\text{H}_2^+ + e^- \rightarrow \text{H}^+ + \text{H} + e^-$ , but the dissociation rate of  $\text{H}_2^+$  is relatively high and the particle speed of  $\text{H}_2$  is slow. Thus these two reactions are regarded as one reaction in this work. The last three reactions, (cx), (iz) and (rc), represent charge exchange, ionization and recombination, respectively. The rate coefficient of these reactions [12, 13] are denoted by  $\langle\sigma_{d1}v\rangle$ ,  $\langle\sigma_{d2}v\rangle$ ,  $\langle\sigma_{cx}v\rangle$ ,  $\langle\sigma_{iz}v\rangle$  and  $\langle\sigma_{rc}v\rangle$ , respectively.

There are several types of expressions to describe neutral dynamics; Monte Carlo simulation, kinetic equation, fluid equation and diffusion equation. Since the mean-free-path (MFP) of neutral-neutral elastic collision of hydrogen atom, e.g. approximately 2 m for a typical neutral density  $10^{19} \text{ m}^{-3}$  near the divertor plate, is comparable to the plasma size and much longer than the decay length of neutrals [8]. Therefore the diffusion process is negligible in the divertor plasma and also the fluid equation of the neutral gas does not correctly describe the characteristics of the wide range of particle energy such as few eV of dissociation atoms and tens eV of charge exchange atoms. Therefore in this paper, we use simplified kinetic-type equations.

We classify the neutrals into four components;

molecules released from the divertor plate, dissociated atoms from the molecules, charge exchange atoms and recombination atoms. The particle speed of each component is treated as a constant;  $v_m$ ,  $v_d$ ,  $v_{cx}$  and  $v_{rc}$ , respectively. The density of each component is denoted by  $n_m$ ,  $n_d^\pm$ ,  $n_{cx}^\pm$  and  $n_{rc}^\pm$ , respectively. The superscript ‘ $\pm$ ’ corresponds to two components with opposite direction, i.e. positive and negative velocity on  $s$ -coordinate. They have each characteristic temperature, or energy, determined from their sources. The molecule temperature  $T_m$  is the same as that of the divertor plate. The temperature of dissociation atoms is determined from the Frank-Condon dissociation energy, i.e.  $T_d \sim 2.5$  eV. The temperatures of charge exchange and recombination atoms,  $T_{cx}$  and  $T_{rc}$ , are determined from the averaged energy of the generated atoms by each processes over  $s = 0$  to  $l_p$ . The velocity of each component is calculated from the corresponding temperature;  $v_m = \sqrt{T_m/\pi m_i}/\cos\varphi$ ,  $v_d = \sqrt{2T_d/\pi m_i}$ ,  $v_{cx} = \sqrt{2T_{cx}/\pi m_i}$  and  $v_{rc} = \sqrt{2T_{rc}/\pi m_i}$ . The angle of the magnetic field measured from the surface normal on the divertor plate was denoted by  $\varphi$  and used to obtain the equivalent velocity of molecules. This conversion is due to the existence of the difference between the directions of plasma and molecule flows, i.e. parallel to the magnetic field and normal to the surface.

The particle balance equations of neutrals are given by

$$-v_m \frac{dn_m}{ds} = (\langle\sigma_{d1}v\rangle + \langle\sigma_{d2}v\rangle) n_m n_e, \quad (6)$$

$$\pm v_d \frac{dn_d^\pm}{ds} = (2\langle\sigma_{d1}v\rangle + \langle\sigma_{d2}v\rangle) n_m n_e - (\langle\sigma_{iz}v\rangle n_e + \langle\sigma_{cx}v\rangle n_i) n_d^\pm, \quad (7)$$

$$\pm v_{cx} \frac{dn_{cx}^\pm}{ds} = (1 - r_{pl}) \frac{v_{cx} \pm v}{2v_{cx}} \langle\sigma_{cx}v\rangle n_a n_i - (\langle\sigma_{iz}v\rangle n_e + \langle\sigma_{cx}v\rangle n_i) n_{cx}^\pm, \quad (8)$$

$$\pm v_{rc} \frac{dn_{rc}^\pm}{ds} = (1 - r_{pl}) \frac{v_{rc} \pm v}{2v_{rc}} \langle\sigma_{rc}v\rangle n_e n_i - (\langle\sigma_{iz}v\rangle n_e + \langle\sigma_{cx}v\rangle n_i) n_{rc}^\pm, \quad (9)$$

where the total density of hydrogen atoms were denoted by  $n_a \equiv n_d^+ + n_d^- + n_{cx}^+ + n_{cx}^- + n_{rc}^+ + n_{rc}^-$  in Eq. (8). Although electron and ion densities are assumed to be the same in this work, we used  $n_e$  and  $n_i$  to distinguish which density is involved in each atomic process. When hydrogen ions hit the wall surface, recombinations take place and hydrogen molecules are released from the surface uniformly. We assumed that two ions yield a hydrogen molecule and there is no loss. Therefore the boundary conditions of neutrals are given by  $n_{m1}v_m = n_1v_1/2$ ,  $n_{d1}^+ = n_{d1}^-$ ,  $n_{cx1}^+ = n_{cx1}^-$ , and  $n_{rc1}^+ = n_{rc1}^-$  at  $s = l_p$ . The particle loss of hydrogen atoms was introduced as a constant ratio  $r_{pl}$  in Eqs. (8) and (9). We assumed that the main loss of neutrals occurs at the generation of neutral atoms because of their isotropic velocities. We note that each equations, (7)-(9), consists of two equations for positive and negative velocities. Thus Eqs. (6)-(9) represents seven equations for seven groups of neutrals;  $n_m$ ,  $n_d^+$ ,  $n_d^-$ ,  $n_{cx}^+$ ,  $n_{cx}^-$ ,  $n_{rc}^+$  and  $n_{rc}^-$ . The coefficient

of the first terms in the right-hand side of Eq. (8), i.e.  $(v_{cx} \pm v)/2v_{cx}$ , is chosen to satisfy particle number and momentum conservation in the charge exchange hydrogen atoms and ions;  $(v_{cx} + v)/2v_{cx} + (v_{cx} - v)/2v_{cx} = 1$  and  $mv_{cx}(v_{cx} + v)/2v_{cx} - mv_{cx}(v_{cx} - v)/2v_{cx} = mv$ . The coefficient in Eq. (9) is also chosen in the same way. In order to conserve the total energy when  $r_{pl} = 0$ , the temperature  $T_{cx}$  and  $T_{rc}$  are calculated as

$$T_{cx} = \frac{\int_0^{l_p} (T_i + m_i v^2/3) \langle\sigma_{cx}v\rangle n_a n_i ds}{\int_0^{l_p} \langle\sigma_{cx}v\rangle n_a n_i ds}, \quad (10)$$

$$T_{rc} = \frac{\int_0^{l_p} (T_i + m_i v^2/3) \langle\sigma_{rc}v\rangle n_e n_i ds}{\int_0^{l_p} \langle\sigma_{rc}v\rangle n_e n_i ds}. \quad (11)$$

The source terms in the plasma equations (1)-(4) are given by

$$S_n = \langle\sigma_{d2}v\rangle n_m n_e + \langle\sigma_{iz}v\rangle n_a n_e - \langle\sigma_{rc}v\rangle n_i n_e, \quad (12)$$

$$S_p = m_i \langle\sigma_{cx}v\rangle n_i \left[ (n_d^+ - n_d^-) v_d + (n_{cx}^+ - n_{cx}^-) v_{cx} + (n_{rc}^+ - n_{rc}^-) v_{rc} - n_a v \right], \quad (13)$$

$$S_{Ee} = -25^{[eV]} \langle\sigma_{iz}v\rangle n_a n_e, \quad (14)$$

$$S_{Ei} = \frac{3}{2} (\langle\sigma_{iz}v\rangle n_e + \langle\sigma_{cx}v\rangle n_i) \left[ (n_d^+ + n_d^-) T_d + (n_{cx}^+ + n_{cx}^-) T_{cx} + (n_{rc}^+ + n_{rc}^-) T_{rc} \right] + 4.3^{[eV]} \langle\sigma_{d2}v\rangle n_e n_m - \langle\sigma_{cx}v\rangle n_s n_i \left( \frac{3}{2} T_i + \frac{1}{2} m_i v^2 \right), \quad (15)$$

where the energy loss of ionization was included in the energy source term of electron, Eq. (14). Although the ionization energy is 13.6 eV, we included the radiation loss from excited atom in the ionization loss, i.e. 25 eV, because the cross section of excitation is almost the same as that of ionization.

### 3. Results and Discussions

We developed a numerical code to solve the plasma equations, (1)-(5), and the neutral equations, (6)-(9), self-consistently. The plasma equations and neutral equations with negative velocity are integrated from the wall boundary,  $s = l_p$ , and the neutral equations with positive velocity are integrated from the upstream boundary,  $s = 0$ . The integrals are carried out numerically by the fourth order Runge-Kutta method and the step width is changed adaptively. Since the plasma and neutral profiles depend on each other, we obtain solutions by solving plasma and neutral equations iteratively. The total calculation time including the iterations is less than one second on an ordinary PC. The number of boundary grid points in EMC3 code is around ten thousands and thus the total calculation time of all flux tubes reaches two hours. The flux tube model, however, can be solved in parallel quite efficiently. Therefore the calculation time can be reduced to around a minute with the aid of a massively parallel machine. Although iterations will be necessary to take account of interactions

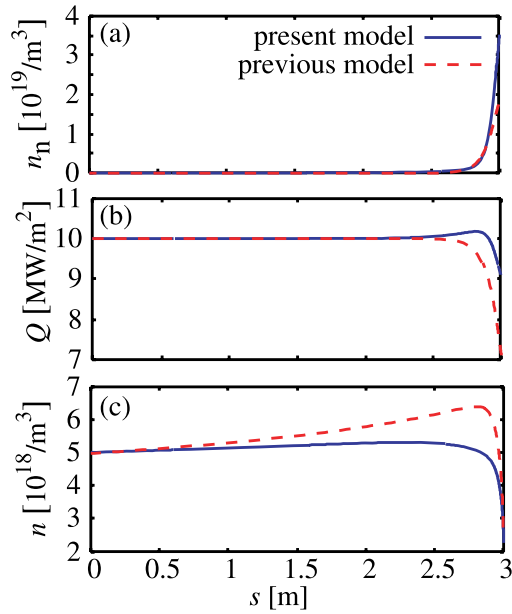


Fig. 2 (a) neutral density, (b) heat flux and (c) plasma density profiles calculated from the present and previous models.

between flux tubes, the total time will be around an hour and less than that of EMC3 code.

In our previous model [8], neutral particles were described simply by density and velocity of one species of hydrogen atom characterized by thermal particles released from wall surface and momentum and energy interactions with the plasma were ignored. Plasma equations and boundary conditions are the same. Comparisons of the solutions between present and previous models are given in Fig. 2. The plasma density and electron and ion heat fluxes at  $s = 0$  are chosen as  $n_0 = 5 \times 10^{18} \text{ m}^{-3}$ ,  $Q_{e0} = Q_{i0} = 5 \text{ MW/m}^2$ . Temperature of the hydrogen molecules, angle of the magnetic field, particle loss ratio and impurity ratio are  $T_m = 600 \text{ K}$ ,  $\varphi = 80^\circ$ ,  $r_{pl} = 0.2$  and  $r_{imp} = 3\%$ , respectively. The global recycling coefficient was calculated as 84% from the particle fluxes at  $s = 0$  and  $l_p$ . A parameter related to the particle loss in the previous model was adjusted to yield the same global recycling coefficient. We note that the sum of the recycling coefficient and the loss rate of neutrals,  $r_{pl}$ , is not unity because the loss rate in Eqs. (8) and (9) represents the loss at the generation of fast neutrals. Therefore the flux multiplication factor depends on the reaction rate of charge exchange and recombination and thus it is not given by  $1/(1 - r_{pl})$ .

The density profiles of hydrogen neutrals,  $n_n = n_a + 2n_m$ , are shown in Fig. 2 (a). The result of the previous model gives lower density near the wall surface because particle loss was underestimated in the previous model. The heat flux  $Q$  of the previous model in Fig. 2 (b) has lower value than that of the present one near the divertor plate. The reason of the difference is due to the overestimate of the energy loss by charge exchange in the previous one. A small peak in front of the wall was observed in the

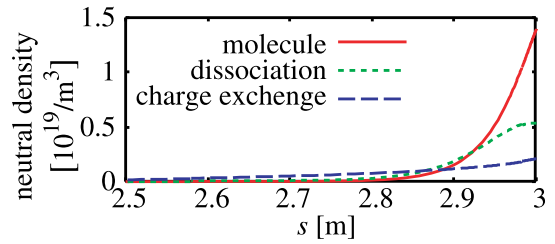


Fig. 3 Density profiles of neutrals; hydrogen molecules, atoms generated by dissociation and charge exchange.

$Q$  profile of the present model. It is caused by the interaction of the ion and neutral energy. High energy neutrals are generated through the charge exchange processes and their energy are transported by the neutral flow. The neutrals remaining in the plasma are ionized and their energy returns to the plasma. Thus the small peak represents energy transport by neutrals from the vicinity of the wall to  $s \sim 2.7 \text{ m}$ . The overestimate of the plasma density in Fig. 2(c) is also caused by the overestimate of the energy loss, or underestimate of the ion temperature.

The density profiles of neutrals near the divertor plate,  $s = 2.5$  to  $3$ , are shown in Fig. 3, where the three curves correspond to their sources; hydrogen molecules released from the wall surface, atoms dissociated from molecules and generated through charge exchange processes. The recombination processes are negligible in this case because the plasma temperature is relatively high. The amount of neutrals corresponding to each source is obtained easily and it is one of advantages of our model. Their densities and decay lengths reflect on the atomic processes and their velocities. Since the molecules and dissociation atoms are relatively slow, their decay length is short,  $\sim 0.1 \text{ m}$  along the magnetic fields, while the charge exchange atoms have longer decay length,  $\sim 0.3 \text{ m}$ , because their characteristic speed is much faster than those of molecules and dissociation atoms. The source profile is also broader because the charge exchange atoms can contribute to new charge exchange processes as a source.

In order to examine dependences of plasma parameters on density, we carried out calculations for different plasma densities with a fixed input heat flux. Boundary values of electron and ion temperatures are shown as functions of plasma density at  $s = 0$  in Fig. 4 (a). Two lines labeled  $T_{e0}$  and  $T_{i0}$  represent the temperatures at upstream boundary,  $s = 0$ , and the others at wall boundary,  $s = l_p$ . Since the input heat flux is fixed to  $Q_{e0} = Q_{i0} = 5 \text{ MW/m}^2$ , temperature becomes low for high density. Electron and ion temperatures tend to be the same near the divertor plate for high density and low temperature case. The temperature drop from  $s = 0$  to  $s = l_p$  becomes large in such case because heat conduction becomes significant to sustain the heat flux in low temperature plasma. The fact that the electron temperature is higher than that of ion in any cases indicates existence of an energy channel from electron to ion

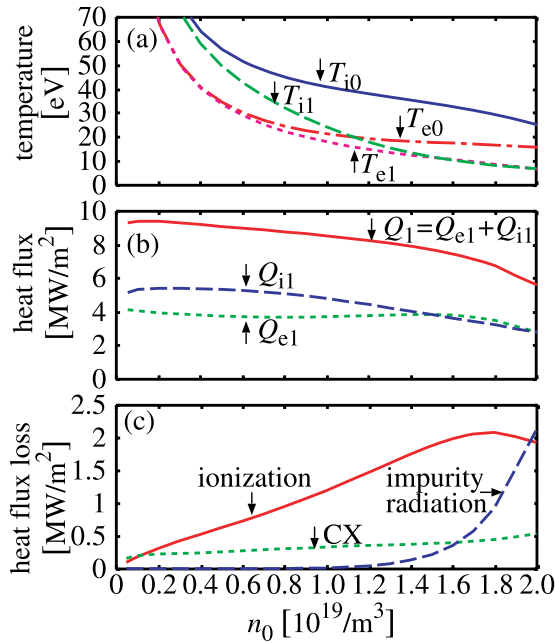


Fig. 4 (a) temperature at  $s = 0$  and  $s = l_p$ , (b) heat flux at the divertor plate, (c) heat flux loss as functions of plasma density at upstream boundary  $n_0$ . Electron, ion and total heat fluxes were denoted by  $Q_e$ ,  $Q_i$  and  $Q$ .

due to collisions.

The heat fluxes at the divertor plate,  $s = l_p$ , are shown as functions of the upstream density in Fig. 4 (a). The electron, ion and total heat fluxes were denoted by  $Q_{e1}$ ,  $Q_{i1}$  and  $Q_1$ , respectively. We note that the actual heat flux on the divertor plate is much smaller than the value  $Q_1$  because it represents the heat flux along the magnetic fields and several times larger than the heat flux normal to the wall. When the density is relatively low, e.g.  $n_0 < 10^{19} \text{ m}^{-3}$ , almost all heat flux coming from the upstream boundary deposits on the divertor plate, while in high density case the heat flux decreases significantly. The contributions of three main energy sinks to the heat flux are compared in Fig. 4 (b). The largest energy loss is caused by radiation due to the electron impact ionization. The loss caused by impurity radiation increases in high density case because the electron temperature decrease below 10 eV, while the charge exchange loss does not change significantly. The loss of neutrals takes place when they are generated through charge exchange processes in this model. Since the input heat flux is fixed, increase of density yields decrease of temperature, or particle energy of the neutrals. Thus the charge exchange loss is not sensitive to the plasma density.

From above discussions we can identify the energy transfer channels in Fig. 5. In low density case,  $n_0 \sim 5 \times 10^{18} \text{ m}^{-3}$ , electron and ion energies are lost by ionization loss and charge exchange loss, respectively. The each amount of the loss is comparable and much smaller than the total heat flux coming from the upstream plasma.

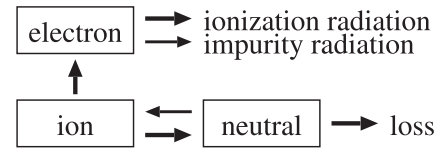


Fig. 5 Schematic diagram of energy channels and flows in the divertor plasma.

In high density case,  $n_0 > 1 \times 10^{19} \text{ m}^{-3}$ , ionization and impurity losses increases and the plasma energy is lost through the electron channel mainly. The impurity cooling increases more rapidly than ionization for  $n_0 > 1.5 \times 10^{19} \text{ m}^{-3}$ .

## 4. Conclusions

A fluid model of LHD divertor plasma and a neutral model were presented. Atomic processes such as dissociation and ionization of hydrogen molecules and atoms were included. We developed a numerical code which has boundary conditions relevant to code connections at the both end of the calculation region, i.e.  $s = 0$  and  $l_p$ . The self-consistent solutions were obtained by iterative calculations of the plasma and neutral equations. The calculation time is less than one second and it is reasonably short for integrated simulation of future studies.

Comparisons of heat flux, neutral and plasma density profiles between the previous [8] and present models were carried out. By treating the interaction of energy between plasma and neutrals directly, the amount of energy loss due to the energetic neutral atoms are included correctly in the model, and thus the overestimate of the energy loss is corrected. Also the profile of each neutral component can be obtained easily from the solution of the model; hydrogen molecules released from the wall, atoms dissociated from molecules and generated through charge exchange processes. They have their own characteristic speed and atomic processes, and thus different profiles were obtained. The molecules have a peaked profile at the wall surface and the charge exchange atoms have long decay length.

The dependence of the heat flux on the plasma density was studied by using the code. In the low density case, the plasma loses its energy by ionization and charge exchange, but effect of the loss on the heat flux is small. On the other hand, for the high density case the ionization loss and impurity cooling becomes large and the heat flux decreases by 40% when the plasma density at the upstream boundary is  $2 \times 10^{19} \text{ m}^{-3}$ . We confirmed that the ion energy is transferred to electron and it is lost by ionization and impurity radiation.

In the paper, we employed constant impurity ratio. The dynamics of impurities is important to obtain the impurity profiles and to elucidate the role of the divertor plasma on the core plasma. Implementation of a fluid impurity model and the application of the model to the integrated simulation are future issues.

## Acknowledgments

The authors would like to thank Dr. T. Takizuka of Japan Atomic Energy Agency for helpful comments. The contribution of the last author was carried out under the European Fusion Development agreement, supported by the European Communities. The views and opinions expressed herein do not necessarily reflect those of the European Commission.

- [1] N. Oyabu *et al.*, Nucl. Fusion **34**, 387 (1994).
- [2] M. Kobayashi *et al.*, J. Nucl. Mater. **363-365**, 294 (2007).
- [3] A. Kirschner *et al.*, Nucl. Fusion **40**, 989 (2000).
- [4] P. C. Stangeby and J. D. Elder, J. Nucl. Mater. **196-198**, 258 (1992).
- [5] K. Shimizu *et al.*, J. Nucl. Mater. **196-198**, 476 (1992).
- [6] Rajiv Goswami *et al.*, Phys. Plasmas **8**, 857 (2001).
- [7] Deok-Kyu Kim and Sanh Hee Hong, Phys. Plasmas **12**, 062504 (2005).
- [8] G. Kawamura, Y. Tomita, M. Kobayashi and A. Kirschner, J. Plasma Fusion Res. Series **8**, 455 (2009).
- [9] S. I. Braginskii, Rev. Plasma Phys. **1**, 205 (1965).
- [10] D. Tskhakaya and S. Kuhn, Plasma Phys. Control. Fusion **47**, A327 (2005).
- [11] Peter C. Stangeby, *The Plasma Boundary of Magnetic Fusion Devices*, Institute of Physics Publishing (Bristol and Philadelphia 1999).
- [12] R. L. Freeman and E. M. Jones, *Atomic Collision Processes in Plasma Physics Experiments*, Culham Laboratory, Abingdon, England, Report CLM-R 137 (1974).
- [13] E. M. Jones, *Atomic Collision Processes in Plasma Physics Experiments*, Culham Laboratory, Abingdon, England, Report CLM-R 175 (1977).